ACS APPLIED MATERIALS & INTERFACES

Research Article

Cite This: ACS Appl. Mater. Interfaces 2018, 10, 36352−36360

www.acsami.org

Thermal Conductivity of Polyacrylamide Hydrogels at the Nanoscale

Shuai Xu,[†,‡] Shengqiang Cai,[‡] and Zishun Liu*[,†]

[†]International Center for Applied Mechanics, State Key Laboratory for Strength and Vibration of Mechanical Structures, Xi'an Jiaotong University, Xi'an 710049, China

[‡]Mechanical and Aerospace Engineering, University of California, San Diego, La Jolla, California 92093, United States

Supporting Information

ABSTRACT: A polymer network can imbibe copious amounts of water and swell, and the resulting state is known as a hydrogel. In many potential applications of hydrogels, such as stretchable conductors, ionic cables, and neuroprostheses, the thermal conductivities of hydrogels should be understood clearly. In the present work, we build molecular dynamics (MD) models of random cross-linked polyacrylamide hydrogels with different water volume fractions through a reaction method. On the basis of these models, thermal conductivities of hydrogels at the nanoscale are investigated by a none-equilibrium MD method. This work reveals that when the water fraction of hydrogels is under 85%, the thermal conductivity increases with the water fraction, and can be even higher than the thermal conductivities of both pure polymer networks and pure water because of the influence of the interface between polymer networks and water. However, when the water fraction in hydrogels is bigger than 85%, its thermal conductivity will decrease and get close to the water's conductivity. Accordingly, to explain this abnormal phenomenon, a 2-order-3-phase theoretical model is proposed by considering hydrogel as a 3-phase composite. It can be found that the proposed theory can predict results which agree quite well with our simulated results.

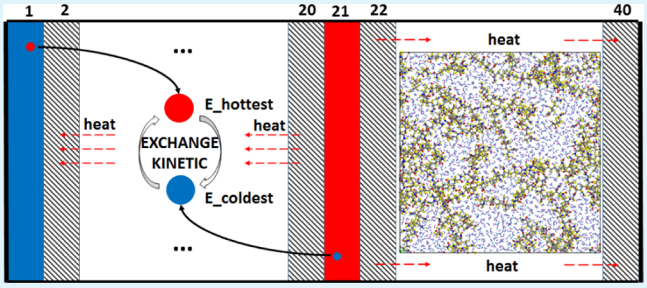

KEYWORDS: *hydrogel, modeling by a reaction method, none-equilibrium molecular dynamics, thermal conductivity, 2-order-3-phase model*

1. INTRODUCTION

A long-chain, flexible polymer can be cross-linked by covalent bonds and form a 3D network. On contact with a suitable solvent, the 3D network can imbibe the solvent and swells, resulting in a material known as polymer gel. If the solvent is water, we call it a hydrogel. Meanwhile, when environment stimuli (such as temperature, pH, and electric field) change, the solvent in the hydrogel migrates out and evaporates, making the swelling process reversible.[1] The hydrogel has attributes of both solid and liquid, that is, elastic deformation results from strong chemical cross-linking between the long-chained polymers, and viscous migration results from the weak physical interaction between the solvent molecules and the long-chained polymers. The combination of the attributes makes hydrogels great potential materials for various applications, such as medical devices,[2,3] tissue engineering,[4,5] actuators responsive to physiological cues,[6−8] and packers in oil wells.[9]

Except for these applications, there are several front research areas about hydrogels. One is using hydrogels as stretchable conductors or ionic cables,[10−14] which could be used in soft electronic devices and soft robots. Another area is neuroprostheses, which use hydrogels as neural tissues.[15] In all these applications, the heat generation, thermal conduction, and thermal match between prostheses and the human body must be considered. Existing thermal research involving hydrogels mainly focused on their nanocomposites[16−18] and their thermal stabilities,[19−21] which pay attention to the role of nanofillers. Illeperuma et al. use hydrogel-fabric laminates as a fire-resistant material.[22] Zhang et al. report a fast thermal response hydrogel composite which can be used as a smart switch.[23] Jiang et al. report a self-healable thermal interface material base on boron nitride nanosheets and cross-linked hydrogel composite,[24] whereas Wu et al. apply a double network hydrogel as a thermistor base on its self-healing property.[25] However, the fundamental study about the thermal conduction in hydrogels, especially at the nanoscale, is in its infancy stage. In-depth understanding and systematic research of the thermal transport mechanism in hydrogels are required.

When studying these thermal-related issues in the above applications, the effect of the interface must be considered, and some of them are even under the microscale. Hence, it is hard to study them through traditional experimental methods. However, molecular dynamics (MD) may provide a good approach to probe these problems, as it could provide the detailed structures and dynamics information of the system at

Received: June 16, 2018
Accepted: September 25, 2018
Published: September 25, 2018

DOI: 10.1021/acsami.8b09891
ACS Appl. Mater. Interfaces 2018, 10, 36352−36360

the molecular level.[26] To ensure the accuracy of MD simulation results, it is necessary to build a reasonable model of hydrogel microstructure. In the present work, we build MD models of a random cross-linked polyacrylamide (PAAm) hydrogel with different water volume fractions by a reaction method. Our model contains a random polymer network and randomly distributed water molecules. Meanwhile, except for the cross-linked main framework, our polymer network model also contains branches, physical cross-links, short chains, and unreacted units, which can reflect the characteristics of the real hydrogel well. On the basis of our MD models, the thermal conductivities of the PAAm hydrogel with different water volume fractions are investigated at the nanoscale by a none-equilibrium MD (NEMD) method. In addition, we propose a 2-order-3-phase theoretical model by considering hydrogel as a 3-phase composite.

2. MODEL AND METHODS

2.1. Modeling of Cross-Linked PAAm Hydrogel. Hydrogels are composed of water and a cross-linked polymer network with a random configuration. It is essential to build its MD model with these characteristics. In this paper, we focus on the PAAm hydrogel. The molecular structures of acrylamide (repeat unit) and *N*,*N*′-methylenediacrylamide (cross-linker) are as shown in Figure 1a,b,

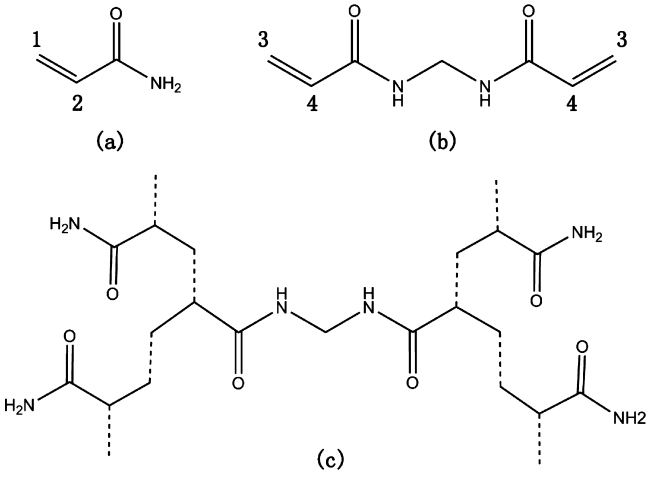

Figure 1. (a) Acrylamide, the repeat unit. (b) *N*,*N*′-Methylenediacrylamide, the cross-linker. (c) Cross-linked PAAm. The dashed short lines mean the C−C bonds generated during the reaction.

respectively. They have been widely used to prepare the PAAm hydrogel.[22,27] The polymer networks are built by simulating the reaction of repeat units and cross-linkers. In Figure 1, the C═C bond may turn into a C−C bond during the reaction; as a result, atoms 1−4 may connect to other C atoms numbered as 1−4 in another repeat unit or cross-linker by a C−C bond and form the cross-linked structure in Figure 1c.

In our simulation, we packed 333 repeat units and 22 cross-linkers into a block region whose dimensions are 5 nm × 5 nm × 1.5 nm as shown in Figure 2a. The initial density is 1.2 g/cm^3. Then, this model was relaxed under the isothermal-isobaric (NPT) ensemble for 50 ps by a large-scale atomic/molecular massively parallel simulator (LAMMPS) using a consistent valence Force Field (CVFF),[28] after which we added C−C bonds between these atoms numbered as 1−4 if their distances were under 5 Å. It should be noticed that this distance value is simply chosen to connect C atoms and form the cross-linked MD model. It is without any chemical meanings and can be any other value. Following this, more "relaxation & connecting" processes were carried out until most of the repeat units and cross-linkers were connected. After the reaction process, the connected

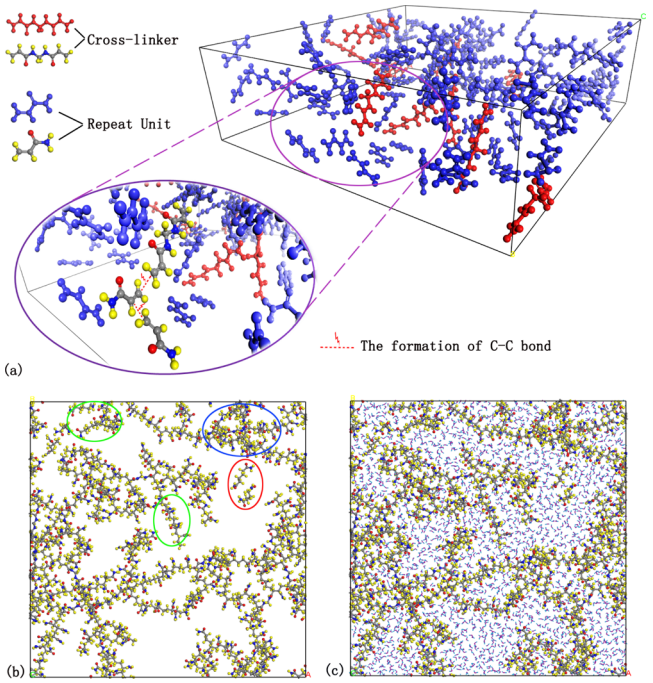

Figure 2. (a) Modeling of the 3D PAAm network by a reaction method. (b) MD model of the PAAm network after a stretch. The blue, green, and red circles represent the physical cross-link, branch chains, and unreacted units, respectively. (c) Hydrogel model with a water volume fraction of 64.98%.

structure was optimized in Material Studio. The final density of the cross-linked network is 1.137 g/cm^3. To see the cross-linked network more clearly, we display it in Figure 2b after a stretching. Under different stretch ratios, we packed water molecules into the network and get hydrogels with different water volume fractions. For example, Figure 2c shows a hydrogel model whose water volume fraction is 64.98%. As demonstrated in Figure 2b,c, except for the cross-linked main framework, our model also contains branches (green circles), physical cross-links (blue circle), and short chains or unreacted units (red circle). Besides, the average density of the PAAm hydrogel we measured in the laboratory is 1.0300 ± 0.0190 g/cm^3 when the water volume fraction is between 40 and 70%, which is almost same as our MD models (1.0725 ± 0.0311 g/cm^3). Therefore, our MD model is quite similar to the real hydrogel structure and has representativeness.

2.2. NEMD Method. On the basis of the NEMD method, which has been widely employed to obtain the thermal conductivities of different materials,[29−32] the thermal conductivity of the hydrogel is determined using LAMMPS. The CVFF force field (details are given in eq S1 and Tables S1−S4) is adopted to simulate interatomic interactions for the whole system. In all of our simulations, the time step is 1 fs. Figure 3 shows the schematic procedures of our simulation using the NEMD method. We first make a copy of the hydrogel model in Figure 2c along the *x*-direction followed by a 100 ps relaxation under the NPT ensemble. Then, the model is separated into 40 slabs. The 1st and 21st are the cool slab and the hot slab, respectively. During the simulation, the hottest atom in the cool slab and the coldest atom in the hot slab would exchange kinetic energy with each other every *N* steps. This can be regarded as pulling out some heat from the cool slab and injecting the same heat into the hot slab, equal to generating a heat flux along the *x*-direction. With a smaller *N*, the heat flux would be bigger. The heat can be expressed as $E_{exchange} = E_{hottest} - E_{coldest}$.

The temperature in each slab is calculated by the following formula

$$T_k = \frac{1}{3n_k k_B} \sum_{i \in k}^{n_k} m_i v_i^2 \quad (1)$$

DOI: 10.1021/acsami.8b09891
ACS Appl. Mater. Interfaces 2018, 10, 36352−36360

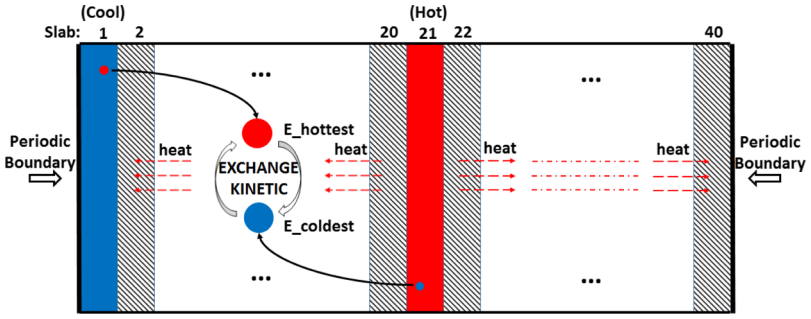

Figure 3. Schematic about the NEMD method.

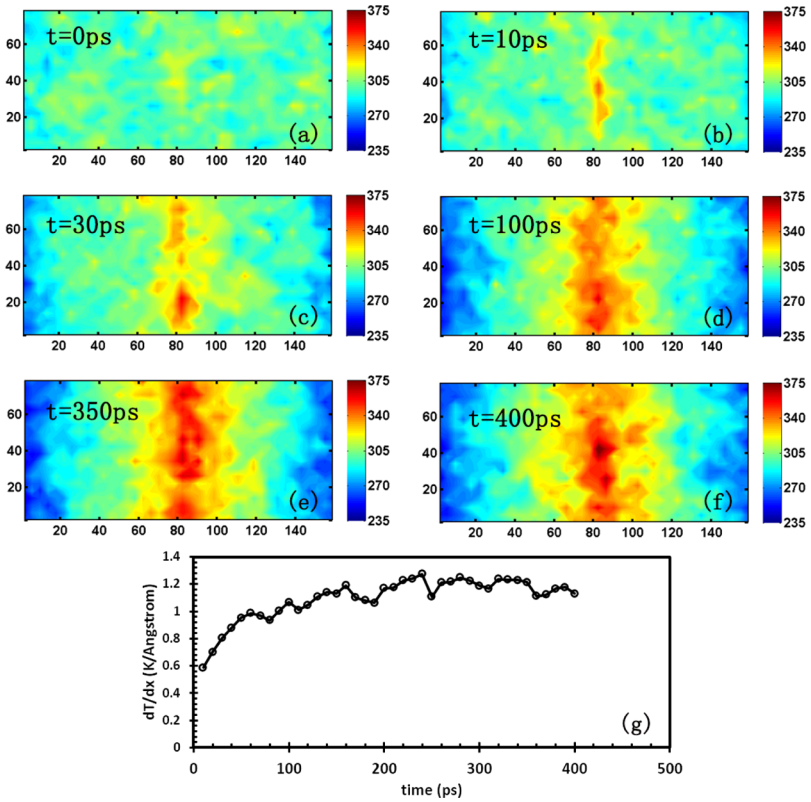

Figure 4. (a–f) Thermal images (temperature distribution, T [K], in the hydrogel) at different times. (g) Temperature gradients in the left half side at different times.

where n_k is the number of atoms in the kth part; k_B is the Boltzmann constant; m_i and v_i are the mass and velocity of the ith atom in the kth part, respectively. The temperature in every slab is averaged every 10 ps. The temperature gradient dT/dx can then be determined by the temperature distribution in the hydrogel. Summing the $E_{exchange}$ up during the simulation, we can get the total heat, and we can get the heat flux by the following formula

$$F = \frac{\sum E_{exchange}}{2tL_yL_z} \quad (2)$$

where t means the total simulation time, L_y and L_z mean box lengths in y and z directions, the factor 1/2 arises from the periodic boundary (energy can flow in two directions). According to Fourier's law, the thermal conductivity is

$$K = -\frac{F}{dT/dx} \quad (3)$$

Then, we can get thermal conductivities of the hydrogel with different water volume fractions under different energy exchange velocities.

We first perform a 400 ps NEMD simulation with the constant energy (NVE) ensemble to reach the steady state, after which another 400 ps simulation is carried out to investigate the temperature distribution and thermal flux in the hydrogel. Figure 4 shows the evolvement of thermal images and temperature gradients during the first 400 ps. In the beginning, the whole system is at room temperature with a slight thermal disturbance (Figure 4a). Then, the temperatures rise or fall in the thermal-inject-in zone and thermal-pull-out zone gradually, making the temperature distribution in the system evolve and generate a temperature gradient gradually (Figure 4b–f). Figure 4g demonstrates that temperature gradient stops increasing after about 200 ps, which means 400 ps is long enough for the system to reach its steady state.

3. RESULTS AND DISCUSSION

3.1. Thermal Conductivity of the PAAm Hydrogel by Simulations. The number of steps between energy exchanges represents the energy exchange velocity. For the same amount of time, when this number is bigger, there will be less energy exchanged, which means the heat flux is smaller. In order to

DOI: 10.1021/acsami.8b09891
ACS Appl. Mater. Interfaces 2018, 10, 36352–36360

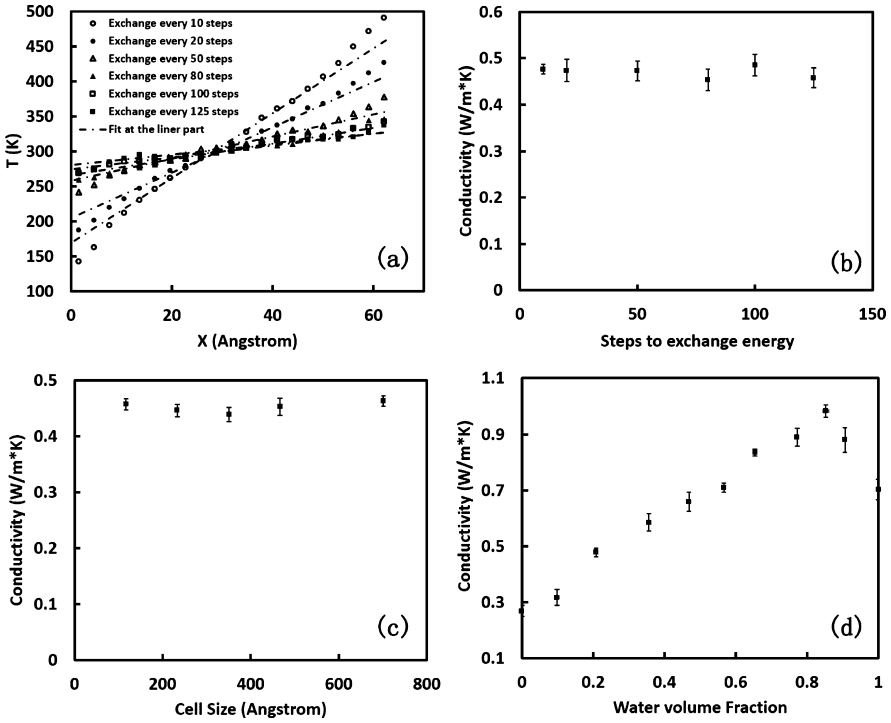

Figure 5. (a) Temperature profiles in the hydrogel (water content is about 20%) with different energy exchange velocities. (b) Thermal conductivity of the hydrogel with different energy exchange velocities. (c) Thermal conductivity of the hydrogel with different cell sizes. (d) Thermal conductivities of the hydrogel with different water volume fractions.

investigate the dependence of conductivities on the heat flux when using the NEMD method, we determine the equivalent thermal conductivities of three models whose water volume fraction is about 20% under six different energy exchange velocities (exchange energy every 10 steps, 20 steps, 50 steps, 80 steps, 100 steps, and 125 steps, respectively).

The temperature distribution of the hydrogel is displayed in Figure 5a. The average conductivities for every exchange velocity are calculated by Fourier's law and plotted in Figure 5b. It shows that the results are almost the same for different exchange velocities. Hence, we may conclude that equivalent thermal conductivity is not dependent on the value of steps between exchanges (heat flux). All of our following simulations will be carried out with a constant energy exchange velocity (exchange every 50 steps).

The size effect of the simulation box because of periodic boundary conditions must be considered when using MD to calculate the thermal conductivity. When the simulation is conducted in a small box, phonons will get scattered more frequently because they re-enter the simulation box before they can be dissipated.[33] In other words, the mean free path of phonons is limited to the order of the simulation cell. This usually makes the thermal conductivity underestimated. In order to obtain the correct thermal conductivity, the dependence of thermal conductivity on cell size is investigated by using different size systems. Two sets of simulations are carried out with cell size changing from about 120 to 700 Å (all of our simulations in this paper are in this range). The result in Figure 5c demonstrates that the thermal conductivity does not have an obvious dependence on the cell size in this range. In other words, our model sizes in this research are bigger than the mean free path of phonons, making our simulation results reliable.

The equivalent thermal conductivities of the PAAm hydrogel with different water factions are investigated in this paper. The results are shown in Figure 5d. Four sets of simulations with different initial configurations are carried out to extract the average values and standard deviations. Particularly, when water volume fractions are 0 and 1, we can get thermal conductivities of dry polymer networks and water, which are 0.2682 ± 0.0199 and 0.7028 ± 0.0369 W m^{-1} K^{-1}, respectively. Figure 5d shows that when the water volume fraction is under 85%, the thermal conductivity of the hydrogel increases with increasing the water fraction. Interestedly, it can be even higher than the thermal conductivities of both polymer networks and water. However, when the water fraction becomes bigger than 85%, the thermal conductivity will decrease and get close to the water's conductivity. According to thermal-dynamics,[34] for a heat conduction problem with mass transportation (e.g., water diffusion in the hydrogel in this research), heat flux will be not only contributed by the temperature gradient but also affected by this mass diffusion phenomenon. Besides, for the same heat flux, the temperature distribution will be affected by the mass transportation. After dividing the water molecules in our hydrogel model into 13 parts according to their distances to the polymer network as shown in Figure 6a, we average their displacement in 1 ps in every part. Particularly, the average displacement of pure water is also investigated. The results shown in Figure 6b indicate that the closer the water molecules come to the polymer network, the more difficult they are to diffuse. When the distance between water and the polymer is big enough, the average displacement of water molecules will converge to the value of pure water. This is because the acylamino ($-CONH_2$) in PAAm is a hydrophilic group. When water molecules are closer to the PAAm network, the interactions between the polymer and water molecules would be stronger and restrict

DOI: 10.1021/acsami.8b09891
ACS Appl. Mater. Interfaces 2018, 10, 36352−36360

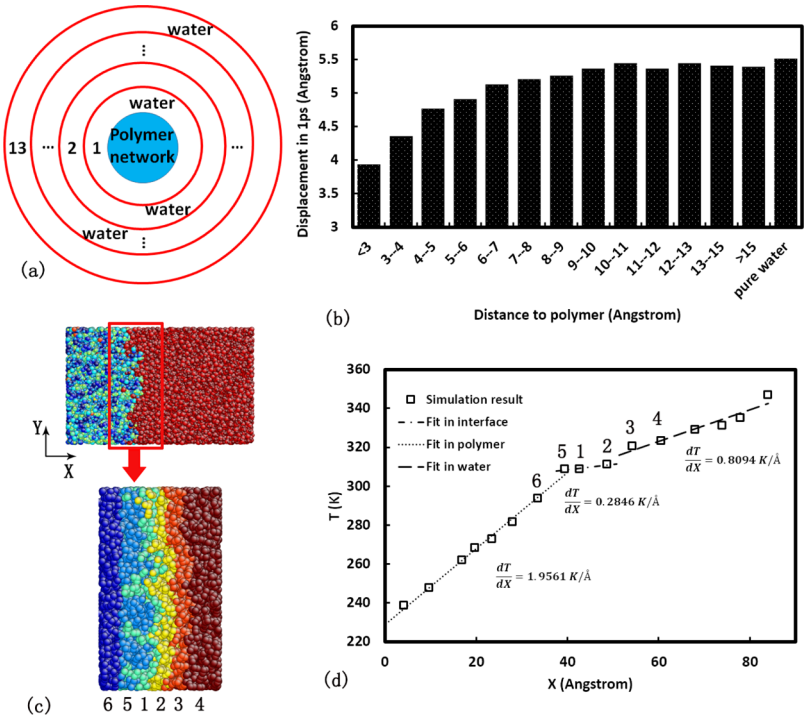

Figure 6. (a) Divide water molecules in the hydrogel into 13 parts according to their distance to the polymer network. (b) Diffusion properties of water molecules in the 13 parts and in pure water. (c) Interface model which contains a polymer layer and a water layer. (d) Temperature distribution in the interface model.

the motion of water. Therefore, the equivalent thermal conductivities of water calculated by Fourier's law (eq 3) may vary according to their distances to the polymer network.

We have built another model containing a polymer layer and a water layer illustrated in Figure 6c to investigate the temperature distribution around and far away from the interface of the polymer and water. Figure 6c only shows the left half side of the model. The cool slab and the hot slab are at the left side and right side, respectively. By the NEMD method, we plot the temperature distribution along the *x*-direction in Figure 6d. Here, we particularly focus on the temperature in six slabs near the water−polymer interface (numbered as 1−6 in Figure 6c,d). Slabs 1−3 are defined as water molecules whose distances to the polymer are 0−3.5, 3.5−7, and 7−11 Å, respectively. Slab 4 is a thin water slab next to 3. Slab 5 is defined as polymer molecules close to water, whereas slab 6 is the polymer slab next to slab 5 with a width of 5 Å. The simulation results shown in Figure 6d can be clearly divided into three parts according to their temperature gradients. With three interface models (the temperature profiles of the other models are displayed in Figure S1), the average conductivities in these three parts are calculated. In the left and right parts, the average conductivities are 0.2841 ± 0.0197 and 0.6732 ± 0.0341 W m^{-1} K^{-1}, respectively, which are consistent with the conductivities of the polymer and free water in Figure 5d. However, the average conductivity of water in slabs 1 and 2 is 2.0139 ± 0.0414 W m^{-1} K^{-1}, which is much higher than that of free water. Hence, we define the water molecules in the hydrogel whose distances to the polymer network are smaller than 7 Å as a new phase. In this paper, we call it the "interface phase". We call the water molecules in the hydrogel whose distances to the polymer are bigger than 7 Å the "free-water phase". Except for these two phases, there is another phase in the hydrogel, which we define as the "polymer phase". When comparing our results with Tang's experimental results,[27] we find the thermal conductivities they investigated (increase from 0.41 to 0.57 W m^{-1} K^{-1} when the water mass fraction increases from 23 to 88%) are smaller than ours. One reason causing this difference may be the resistance between the heater and sample in their tests. Another reason is that the interface between the network and water would have a great influence on the thermal conductivity at the nanoscale in our calculations as discussed above, whereas their tests are carried out at the macroscale. In the next section, we will try to build a theoretical model based on these three phases.

3.2. 2-Order-3-Phase Theoretical Model. In this study, we take the hydrogel as a composite (regard the free-water, interface, and polymer as three phases of the composite). As the free-water is always surrounded by the interface, here we will first build the theoretical model for free-water and interface by taking them as a cluster-filled composite. Generally, we consider a case in which phase 1 is surrounded by phase 2 which is in turn surrounded by another material. Here, we suppose phase 1 and phase 2 are spherical with radii r_1 and r_2, respectively. The equivalent thermal conductivity K of phase 1 and phase 2 is determined by the condition that the temperature distribution outside r_2 would be unaffected if the material inside r_2 is replaced by a material whose conductivity equals K. According to Maxwell,[35] let the temperature, both in phase 1 and phase 2, be expanded in harmonics S_i

$$T_1 = (a_i r^i + b_i r^{-(i+1)})S_i, \qquad r < r_1 \tag{4}$$

$$T_2 = (c_i r^i + d_i r^{-(i+1)})S_i, \qquad r_1 < r < r_2 \tag{5}$$

where a_i, b_i, c_i, and d_i are constants, and S_i does not depend on r. Here, we suppose that there is no source of heat in phase 1 and phase 2, there will be no infinite values of T, and we shall

DOI: 10.1021/acsami.8b09891
ACS Appl. Mater. Interfaces 2018, 10, 36352−36360

have $b_i = 0$. As the most important term in the harmonic expansion is that in which $i = 1$, eqs 4 and 5 can be rewritten as

$$T_1 = arS, \qquad r < r_1 \tag{6}$$

$$T_2 = \left(cr + \frac{d}{r^2}\right)S, \qquad r_1 < r < r_2 \tag{7}$$

At the interface of phase 1 and phase 2, where $r = r_1$, temperatures in phase 1 and phase 2 must be the same, and the flux flow out of phase 1 must equal the flux flow into phase 2. Therefore, we must have

$$T_1 = T_2 \text{ and } K_1\frac{\partial T_1}{\partial r} = K_2\frac{\partial T_2}{\partial r} \tag{8}$$

where K_1 and K_2 are conductivities of phase 1 and phase 2, respectively. From eqs 6−8 we get

$$\left.\begin{aligned} c &= \frac{K_1 + 2K_2}{3K_2}a \\ d &= \frac{K_2 - K_1}{3K_2}r_1^3 a \end{aligned}\right\} \tag{9}$$

We also let the temperature T_3 outside r_2 be expanded in harmonics S_i, and only consider the first term

$$T_3 = f(r)S \tag{10}$$

where f is a function of r, and we do not care about its exact form. Similar to eq 8, where $r = r_2$, we must have

$$T_2 = T_3 \text{ and } K_2\frac{\partial T_2}{\partial r} = K_3\frac{\partial T_3}{\partial r} \tag{11}$$

in which K_3 is the conductivity of the material outside r_2. From eqs 7, 10, and 11 we get

$$\left.\begin{aligned} c + \frac{d}{r_2^3} &= \frac{f(r_2)}{r_2} \\ K_2\left(c - 2\frac{d}{r_2^3}\right) &= K_3\frac{\mathrm{d}f}{\mathrm{d}r} \end{aligned}\right\} \tag{12}$$

If we consider materials inside r_2 as a whole system with an equivalent conductivity K. Similar to eq 6, suppose the temperature distribution inside r_2 is

$$T_{1\&2} = ArS, \qquad r < r_2 \tag{13}$$

The temperature distribution outside r_2 should not be affected and still be described by eq 10. At $r = r_2$ we still have

$$T_{1\&2} = T_3 \text{ and } K\frac{\partial T_{1\&2}}{\partial r} = K_3\frac{\partial T_3}{\partial r} \tag{14}$$

From eqs 10, 13, and 14 we have

$$\left.\begin{aligned} A &= \frac{f(r_2)}{r_2} \\ KA &= K_3\frac{\mathrm{d}f}{\mathrm{d}r} \end{aligned}\right\} \tag{15}$$

Let $\nu_1 = (r_1/r_2)^3$ and $\nu_2 = 1 - \nu_1$, which represent the volume fractions of phase 1 and phase 2 inside r_2, respectively. According to eqs 9, 12, and 15, we obtain the equivalent conductivity of system inside r_2

$$K = K_2\frac{\nu_2 + \nu_1\frac{3K_1}{K_1 + 2K_2}}{\nu_2 + \nu_1\frac{3K_2}{K_1 + 2K_2}} \tag{16}$$

If we regard the free-water as phase 1 and the interface as phase 2, according to eq 16, the equivalent thermal conductivity of water in the hydrogel, K'_w, can be written as

$$K'_w = K_i\frac{3K_w - 2\nu_{i-w}(K_w - K_i)}{3K_i + \nu_{i-w}(K_w - K_i)} \tag{17}$$

where K_w and K_i are thermal conductivities of free-water and interface, ν_{i-w} is the fraction of water molecules in interface, and can be written as

$$\nu_{i-w} = \frac{V_i}{V_w} \tag{18}$$

in which V_i and V_w are the volume of the interface and total water, respectively.

According to Eucken[36] and Brailsford,[37] the single-cluster model above may easily be extended to determine the thermal conductivity of a mixture in which two different kinds of clusters (cluster 1 and cluster 2) are randomly embedded in material 0. By considering the region around "1" cluster, eq 16 can be rewritten as

$$K = K_0\frac{f_1\nu_0 + \nu_1\frac{3K_1}{K_1 + 2K_0}}{f_1\nu_0 + \nu_1\frac{3K_0}{K_1 + 2K_0}} \tag{19}$$

where f_1 is the fraction of material 0 surrounding cluster 1. Solving this equation for f_1, we have

$$f_1 = \frac{3K_0\nu_1\frac{K_1 - K}{K_1 + 2K_0}}{\nu_0(K - K_0)} \tag{20}$$

Similarly, considering the region around "2" clusters, an equation similar to (20) can be obtained with suffix 1 replaced by suffix 2. As $f_1 + f_2 = 1$ must be satisfied, we obtain thermal conductivity of the mixture of materials 0, 1, and 2

$$K = K_0\frac{\nu_0 + \nu_1\frac{3K_1}{K_1 + 2K_0} + \nu_2\frac{3K_2}{K_2 + 2K_0}}{\nu_0 + \nu_1\frac{3K_0}{K_1 + 2K_0} + \nu_2\frac{3K_0}{K_2 + 2K_0}} \tag{21}$$

Consider such a case, in which a random 2-phase assembly (phase 1 and phase 2) is embedded in material 0 and material 0 is totally same with the 2-phase assembly. This means in eq 21, $K_0 = K$ and $\nu_0 = \nu_1 + \nu_2 = 1$. Then, we can get

$$\nu_1\frac{K_1 - K}{K_1 + 2K} + \nu_2\frac{K_2 - K}{K_2 + 2K} = 0 \tag{22}$$

This equation should give the thermal conductivity of a 2-phase composite in which each phase is treated completely equivalently. This is suitable for the random mixture of polymer and water in the hydrogel.

Combining eqs 17 and 22, we can obtain a "2-order-3-phase model" for the hydrogel as shown in eq 23

DOI: 10.1021/acsami.8b09891
ACS Appl. Mater. Interfaces 2018, 10, 36352−36360

$$\left.\begin{aligned} K'_{\mathrm{w}} &= K_{\mathrm{i}}\frac{3K_{\mathrm{w}} - 2\nu_{\mathrm{i-w}}(K_{\mathrm{w}} - K_{\mathrm{i}})}{3K_{\mathrm{i}} + \nu_{\mathrm{i-w}}(K_{\mathrm{w}} - K_{\mathrm{i}})}, && \text{first order} \\ (1-\nu_{\mathrm{w}})\frac{K_{\mathrm{p}} - K_{\mathrm{h}}}{K_{\mathrm{p}} + 2K_{\mathrm{h}}} &+ \nu_{\mathrm{w}}\frac{K'_{\mathrm{w}} - K_{h}}{K'_{\mathrm{w}} + 2K_{\mathrm{h}}} = 0, && \text{second order} \end{aligned}\right\} \quad (23)$$

in which K_{h} is the hydrogel's thermal conductivity, K_{p} is the conductivity of the polymer, and ν_{w} is the total volume fraction of water in the hydrogel. The three phases in our model are polymer, interface, and free-water, respectively. In the first order, we consider water as a cluster-filled composite and get its fuivalent thermal conductivity. In the second order, we regard the mixture of the polymer and water as a random 2-phase composite. The two phases are treated completely equivalently, which we think is more suitable for the hydrogel. By solving eq 23, we can obtain K_{h} as a function of $\nu_{\mathrm{i-w}}$ and ν_{w}. However, it is hard to get $\nu_{\mathrm{i-w}}$, whereas ν_{w} can be easily determined by comparing the hydrogel's volume with its volume at dry state. This may encourage us to establish a relationship between $\nu_{\mathrm{i-w}}$ and ν_{w}. In the first-order model, we know the width of phase 2 (interface) is d = 7 Å. Hence, we have $r_2 = r_1 + d$. Then, according to eq 18, we obtain

$$\nu_{\mathrm{i-w}} = \frac{V_{\mathrm{i}}}{V_{\mathrm{w}}} = \frac{{r_2}^3 - (r_2 - d)^3}{{r_2}^3} = 1 - \left(1 - \frac{d}{r_2}\right)^3 \quad (24)$$

With some simple mathematical procedures, we can get

$$\frac{d}{r_2} = \frac{d}{\sqrt[3]{V}}\frac{\sqrt[3]{V}}{r_2} \quad (25)$$

where V is the volume of the hydrogel, and we have

$$V = \frac{V_{\mathrm{p}}}{1 - \nu_{\mathrm{w}}} = \frac{\frac{4}{3}\pi {r_2}^3}{\nu_{\mathrm{w}}} \quad (26)$$

in which V_{p} is the volume of dry state and can be easily determined. In our cases, $V_{\mathrm{p}} \approx 37\,800$ Å^3. From eqs 24−26, we obtain

$$\nu_{\mathrm{i-w}} = 1 - \left(1 - d \times \sqrt[3]{\frac{4\pi(1-\nu_{\mathrm{w}})}{3\nu_{\mathrm{w}}V_{\mathrm{p}}}}\right)^3 \quad (27)$$

Combining eqs 23 and 27, we obtain K_{h} as a function of only ν_{w}, and the result is shown in Figure 7 as the solid line. Our theoretical result has good agreement with our simulation results, and can well catch the high conductivities when the water fraction is around 85%. This means, in some applications of hydrogels, we do not have to build a complex experimental system to determine the thermal conductivity. They can be easily got by our model with some basic parameters. We also compare our results with the well-known effective medium theory (EMT) model,[38,39] which gives the thermal conductivity of a random mixed 2-phase composite in Figure 7 as the dashed line. When taking water and the polymer as the two phases, the conductivity given by the EMT model is always much smaller than our simulations and is always between the conductivities of water and polymer. This is because hydrogel cannot be simply regarded as a 2-phase material at the nanoscale. The interface between water and polymer networks must be considered as mentioned in our 2-order-3-phase model. We list the fractions of polymer (V-poly), interface (V-inter), and free-water (V-free) at every water content in Table S5. When the water content is under 76.70%, V-inter and V-free both increase with the increasing of water content, making the equivalent conductivity of hydrogel also increase. When the water content increases from 76.70 to 84.44%, although V-inter decreases a little, the conductivity of hydrogel still keeps increasing because V-poly decreases a lot. On substituting the fractions of the three phases into our analytical model, we can also see the conductivity at 84.44% is higher than the conductivity at 76.70%. When the water content is bigger than 84.44%, V-inter decreases rapidly and the V-free increases rapidly, which makes the conductivity of the hydrogel decrease. This in why the highest thermal conductivity was achieved at a water content of 84.44%. Our simulations and theoretical model may provide us a guidance when applying the hydrogel in those situations where thermal issues must be concerned, such as soft electronic devices and neuroprostheses.

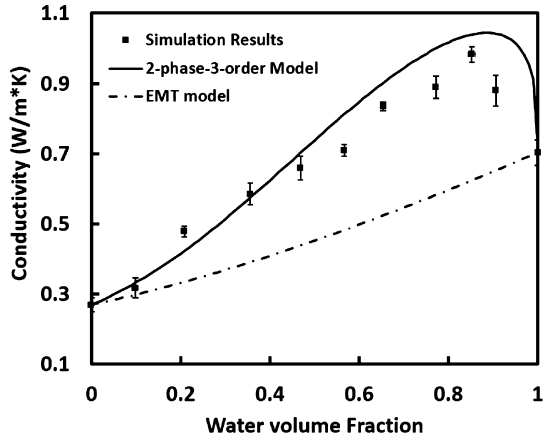

Figure 7. Comparison of our results (MD simulation and 2-order-3-phase model prediction) and the EMT model.

4. CONCLUSIONS

In conclusion, we built the MD model of the PAAm hydrogel by simulating the reaction process of repeat units and cross-linkers. On the basis of our MD models, we investigated the equivalent thermal conductivities of the hydrogel with different water volume fractions at the nanoscale by an NEMD method. Our results show that when the water fraction is under 85%, its equivalent thermal conductivity increases with the water fraction, and can be even higher than the thermal conductivities of both polymer networks and water. However, when the water fraction comes bigger than 85%, its equivalent thermal conductivity will decrease and get close to water's conductivity. After extensive analyses of simulation results, we found that the effect of the interface between water and polymer would be non-negligible at the nanoscale. We further explain the reason why the conductivity of the interface of polymer networks and water is much higher than both pure polymer networks and pure water. Accordingly, to elucidate the finding of our simulations, we further proposed a 2-order-3-phase theoretical model by considering hydrogel as a 3-phase composite to predict our simulation results. Also, we find that our theoretical result has good agreement with our simulations.

DOI: 10.1021/acsami.8b09891
ACS Appl. Mater. Interfaces 2018, 10, 36352−36360

■ ASSOCIATED CONTENT

Supporting Information

The Supporting Information is available free of charge on the ACS Publications website at DOI: 10.1021/acsami.8b09891.

CVFF force field parameters and some simulation results (PDF)

■ AUTHOR INFORMATION

Corresponding Author

*E-mail: zishunliu@mail.xjtu.edu.cn.

ORCID

Shengqiang Cai: 0000-0002-6852-7680

Zishun Liu: 0000-0003-4669-8347

Notes

The authors declare no competing financial interest.

■ ACKNOWLEDGMENTS

S.X. and Z.L. are grateful for the support from the National Natural Science Foundation of China through grant number 11572236.

■ ABBREVIATIONS

MD,molecular dynamics; NEMD,none-equilibrium molecular dynamics; PAAm,polyacrylamide; LAMMPS,large-scale atomic/molecular massively parallel simulator

■ REFERENCES

(1) Liu, Z.; Toh, W.; Ng, T. Y. Advances in Mechanics of Soft Materials: A Review of Large Deformation Behavior of Hydrogels. *Int. J. Appl. Mech. Eng.* **2015**, *07*, 1530001.

(2) Peppas, N. A.; Hilt, J. Z.; Khademhosseini, A.; Langer, R. Hydrogels in Biology and Medicine: From Molecular Principles to Bionanotechnology. *Adv. Mater.* **2006**, *18*, 1345−1360.

(3) Wichterle, O.; Lím, D. Hydrophilic Gels for Biological Use. *Nature* **1960**, *185*, 117−118.

(4) Wong, A. P.; Perez-Castillejos, R.; Christopher Love, J.; Whitesides, G. M. Partitioning microfluidic channels with hydrogel to construct tunable 3-D cellular microenvironments. *Biomaterials* **2008**, *29*, 1853−1861.

(5) Lee, K. Y.; Mooney, D. J. Hydrogels for Tissue Engineering. *Chem. Rev.* **2001**, *101*, 1869−1880.

(6) Dong, L.; Agarwal, A. K.; Beebe, D. J.; Jiang, H. Adaptive Liquid Microlenses Activated by Stimuli-responsive Hydrogels. *Nature* **2006**, *442*, 551−554.

(7) Beebe, D. J.; Moore, J. S.; Bauer, J. M.; Yu, Q.; Liu, R. H.; Devadoss, C.; Jo, B.-H. Functional Hydrogel Structures for Autonomous Flow Control inside Microfluidic Channels. *Nature* **2000**, *404*, 588−590.

(8) Cho, E. C.; Kim, J.-W.; Fernández-Nieves, A.; Weitz, D. A. Highly Responsive Hydrogel Scaffolds Formed by Three-dimensional Organization of Microgel Nanoparticles. *Nano Lett.* **2008**, *8*, 168−172.

(9) Kleverlaan, M.; vanNoort, R. H.; Jones, I. *Deployment of Swelling Elastomer Packers in Shell E&P*; SPE/IADC Drilling Conference: Amsterdam, Netherlands, 2005, p 92346.

(10) Chen, B.; Lu, J. J.; Yang, C. H.; Yang, J. H.; Zhou, J.; Chen, Y. M.; Suo, Z. Highly Stretchable and Transparent Ionogels as Nonvolatile Conductors for Dielectric Elastomer Transducers. *ACS Appl. Mater. Interfaces* **2014**, *6*, 7840−7845.

(11) Yang, C. H.; Chen, B.; Lu, J. J.; Yang, J. H.; Zhou, J.; Chen, Y. M.; Suo, Z. Ionic Cable. *Extreme Mech. Lett.* **2015**, *3*, 59−65.

(12) Keplinger, C.; Sun, J.-Y.; Foo, C. C.; Rothemund, P.; Whitesides, G. M.; Suo, Z. Stretchable, Transparent, Ionic Conductors. *Science* **2013**, *341*, 984−987.

(13) Bai, Y.; Jiang, Y.; Chen, B.; Chiang Foo, C.; Zhou, Y.; Xiang, F.; Zhou, J.; Wang, H.; Suo, Z. Cyclic Performance of Viscoelastic Dielectric Elastomers with Solid Hydrogel Electrodes. *Appl. Phys. Lett.* **2014**, *104*, 062902.

(14) Sun, J.-Y.; Keplinger, C.; Whitesides, G. M.; Suo, Z. Ionic Skin. *Adv. Mater.* **2014**, *26*, 7608−7614.

(15) Minev, I. R.; Musienko, P.; Hirsch, A.; Barraud, Q.; Wenger, N.; Moraud, E. M.; Gandar, J.; Capogrosso, M.; Milekovic, T.; Asboth, L.; Torres, R. F.; Vachicouras, N.; Liu, Q.; Pavlova, N.; Duis, S.; Larmagnac, A.; Voros, J.; Micera, S.; Suo, Z.; Courtine, G.; Lacour, S. P. Electronic Dura Mater for Long-term Multimodal Neural Interfaces. *Science* **2015**, *347*, 159−163.

(16) Iglesias, D.; Bosi, S.; Melchionna, M.; Da Ros, T.; Marchesan, S. The Glitter of Carbon Nanostructures in Hybrid/Composite Hydrogels for Medicinal Use. *Curr. Top. Med. Chem.* **2016**, *16*, 1976−1989.

(17) Mehrali, M.; Thakur, A.; Pennisi, C. P.; Talebian, S.; Arpanaei, A.; Nikkhah, M.; Dolatshahi-Pirouz, A. Nanoreinforced Hydrogels for Tissue Engineering: Biomaterials That Are Compatible with Load-Bearing and Electroactive Tissues. *Adv. Mater.* **2017**, *29*, 1603612.

(18) Zhao, Z.; Fang, R.; Rong, Q.; Liu, M. Bioinspired Nanocomposite Hydrogels with Highly Ordered Structures. *Adv. Mater.* **2017**, *29*, 1703045.

(19) Sun, Y.; Zhou, X.; Liu, Y.; Zhao, G.; Jiang, Y. Effect of Magnetic Nanoparticles on the Properties of Magnetic Rubber. *Mater. Res. Bull.* **2010**, *45*, 878−881.

(20) Koob, T. J.; Hernandez, D. J. Mechanical and Thermal Properties of Novel Polymerized NDGA-Gelatin Hydrogels. *Biomaterials* **2003**, *24*, 1285−1292.

(21) Dash, R.; Foston, M.; Ragauskas, A. J. Improving the Mechanical and Thermal Properties of Gelatin Hydrogels Cross-linked by Cellulose Nanowhiskers. *Carbohydr. Polym.* **2013**, *91*, 638−645.

(22) Illeperuma, W. R. K.; Rothemund, P.; Suo, Z.; Vlassak, J. J. Fire-Resistant Hydrogel-Fabric Laminates: A Simple Concept That May Save Lives. *ACS Appl. Mater. Interfaces* **2016**, *8*, 2071−2077.

(23) Zhang, C.-L.; Cao, F.-H.; Wang, J.-L.; Yu, Z.-L.; Ge, J.; Lu, Y.; Wang, Z.-H.; Yu, S.-H. Highly Stimuli-Responsive Au Nanorods/Poly(N-isopropylacrylamide) (PNIPAM) Composite Hydrogel for Smart Switch. *ACS Appl. Mater. Interfaces* **2017**, *9*, 24857−24863.

(24) Jiang, H.; Wang, Z.; Geng, H.; Song, X.; Zeng, H.; Zhi, C. Highly Flexible and Self-Healable Thermal Interface Material Based on Boron Nitride Nanosheets and a Dual Cross-Linked Hydrogel. *ACS Appl. Mater. Interfaces* **2017**, *9*, 10078−10084.

(25) Wu, J.; Han, S.; Yang, T.; Li, Z.; Wu, Z.; Gui, X.; Tao, K.; Miao, J.; Norford, L. K.; Liu, C.; Huo, F. Highly Stretchable and Transparent Thermistor Based on Self-Healing Double Network Hydrogel. *ACS Appl. Mater. Interfaces* **2018**, *10*, 19097−19105.

(26) Xu, S.; Wang, Y.; Hu, J.; Liu, Z. Atomic Understanding of the Swelling and Phase Transition of Polyacrylamide Hydrogel. *Int. J. Appl. Mech. Eng.* **2016**, *08*, 1640002.

(27) Tang, N.; Peng, Z.; Guo, R.; An, M.; Chen, X.; Li, X.; Yang, N.; Zang, J. Thermal Transport in Soft PAAm Hydrogels. *Polymers* **2017**, *9*, 688.

(28) Dauber-Osguthorpe, P.; Roberts, V. A.; Osguthorpe, D. J.; Wolff, J.; Genest, M.; Hagler, A. T. Structure and energetics of ligand binding to proteins:Escherichia coli dihydrofolate reductase-trimethoprim, a drug-receptor system. *Proteins: Struct., Funct., Bioinf.* **1988**, *4*, 31−47.

(29) Müller-Plathe, F. A Simple Nonequilibrium Molecular Dynamics Method for Calculating the Thermal Conductivity. *J. Chem. Phys.* **1997**, *106*, 6082−6085.

(30) Shen, X.; Lin, X.; Jia, J.; Wang, Z.; Li, Z.; Kim, J.-K. Tunable Thermal Conductivities of Graphene Oxide by Functionalization and Tensile Loading. *Carbon* **2014**, *80*, 235−245.

(31) Bagri, A.; Kim, S.-P.; Ruoff, R. S.; Shenoy, V. B. Thermal Transport Across Twin Grain Boundaries in Polycrystalline Graphene from Nonequilibrium Molecular Dynamics Simulations. *Nano Lett.* **2011**, *11*, 3917−3921.

(32) Shen, X.; Wang, Z.; Wu, Y.; Liu, X.; He, Y.-B.; Kim, J.-K. Multilayer Graphene Enables Higher Efficiency in Improving Thermal Conductivities of Graphene/epoxy Composites. *Nano Lett.* **2016**, *16*, 3585−3593.
(33) Che, J.; Çagin, T.; Goddard, W. A., III Thermal Conductivity of Carbon Nanotubes. *Nanotechnology* **2000**, *11*, 65−69.
(34) De Groot, S. R.; Mazur, P. *Nonequilibrium Thermodynamics*; Dover: New York, 2011; pp 273−284.
(35) Maxwell, J. C. *A Treatise on Electricity and Magnetism*, 3rd ed.; Dover: New York, 1954; Vol. *1*, p 435.
(36) Eucken, A. Allgemeine Gesetzmäßigkeiten für das Wärmeleitvermögen verschiedener Stoffarten und Aggregatzustände. *Forsch. Geb. Ingenieurwes.* **1940**, *11*, 6−20.
(37) Brailsford, A. D.; Major, K. G. The Thermal Conductivity of Aggregates of Several Phases, Including Porous Materials. *Br. J. Appl. Phys.* **1964**, *15*, 313−319.
(38) Böttcher, C. J. F. *Theory of Electric Polarization*; Elsevier: Houston, 1952; pp 415−420.
(39) Landauer, R. The Electrical Resistance of Binary Metallic Mixtures. *J. Appl. Phys.* **1952**, *23*, 779−784.

DOI: 10.1021/acsami.8b09891
ACS Appl. Mater. Interfaces 2018, 10, 36352−36360